Ordering in quasi-two-dimensional planar ferromagnets: A neutron scattering study of graphite intercalation compounds

D. G. Wiesler, M. Suzuki,* and H. Zabel
Department of Physics and Materials Research Laboratory, University of Illinois at Urbana-Champaign, 1110 West Green Street, Urbana, Illinois 61801
(Received 13 February 1987)

The magnetic ordering of stage-2 $CoCl_2$- and $NiCl_2$-graphite intercalation compounds (GIC's) has been investigated by neutron diffraction. Both of these compounds are observed to undergo a two-step ordering process. For temperatures within the range $T_l < T < T_u$ purely two-dimensional (2D) spin correlations are observed, while at temperatures below T_l ferromagnetically aligned planes couple weakly with an average antiferromagnetic interplanar correlation. No three-dimensional long-range magnetic order is observed even at the lowest temperatures attained. The absence of fine structure in scans along (h,k,l) with fixed h and k indicates that successive intercalate layers are translationally uncorrelated from each other. The in-plane peaks of $CoCl_2$-GIC appear to have a shape characteristic of long-range spin order below T_l. However, the structure factor expected for a finite-sized bound vortex phase cannot at present be discounted for $CoCl_2$-GIC. A similar scan at $T_l < T < T_u$ is likewise inconclusive concerning the existence of the bound vortex phase of coplanar spins in the intermediate temperature regime.

I. INTRODUCTION

Magnetic graphite intercalation compounds (GIC's) afford an excellent system for studying the relationship between dimensionality and magnetism. In these compounds, magnetic materials form sheets (the intercalate layer) separated periodically by a number (the stage number) of graphite layers in stacks along the c axis. By increasing the stage number, one should approach ideal two-dimensional (2D) magnetic behavior, and by varying the intercalant species, different types of magnetic interactions may be obtained. Thus magnetic GIC's can be instrumental in the investigation of 2D-3D crossover behavior for a wide variety of materials.

$CoCl_2$- and $NiCl_2$-GIC's, in particular, have attracted a great deal of attention as close approximations to a 2D planar (XY) ferromagnetic spin system. (For recent reviews, see Refs. 1–4.) Such a system is one of a class of 2D systems having a two-component order parameter, whose critical behavior was first elucidated by Kosterlitz and Thouless[5,6] and expanded by José *et al.*[7] and Huber.[8] While it has been rigorously proven[9] that long-range order in these systems does not exist at any temperature $T>0$, there do exist transitions in which the susceptibility and correlation length diverge. These transitions, referred to generally as Kosterlitz-Thouless (KT) transitions, are closely associated with the unbinding of topological defects as the temperature is raised above a critical temperature T_{KT}.

In the case of a 2D XY spin system, these topological defects are spin vortices, which bind together to form vortex pairs of zero net circulation as the system is cooled through T_{KT}. Below T_{KT} the spin-spin correlation function $g(r_{ij})$ behaves asymptotically at large r_{ij} as a power law,

$$g(r_{ij})=\langle \mathbf{S}_i\cdot\mathbf{S}_j\rangle \sim r_{ij}^{-\eta(T)} , \tag{1}$$

instead of the conventional decaying exponential. Fourier-transforming this on a periodic lattice leads to a cusp-shaped structure factor below T_{KT} instead of the usual δ-function Bragg peaks,

$$S_{\mathbf{Q}} \propto \int d^2r\, g(\mathbf{r})\exp(i\mathbf{Q}\cdot\mathbf{r}) \sim |\mathbf{Q}-\mathbf{G}|^{-2+\eta} , \tag{2}$$

where $\mathbf{G}$ is a reciprocal-lattice vector. As T approaches T_{KT} from above, the correlation length ξ diverges faster than the usual power law of the reduced temperature $t=(T-T_{KT})/T_{KT}$. This leads to an exponentially dependent bulk susceptibility,

$$\chi_0 \sim \xi^{2-\eta} \sim \exp[(2-\eta)bt^{-1/2}] , \tag{3}$$

where $b\approx 1.5$ and η is a temperature-dependent critical exponent with a value $\frac{1}{4}$ at T_{KT}.[6]

Kosterlitz-Thouless transitions have been observed in an increasing number of physical systems, including liquid-crystal films,[10] superfluid films of ^{4}He,[11] and planar arrays of Josephson junctions.[12] There is also some evidence now for vortex-type excitations in quasi-2D XY spin systems. In particular, critical scattering of K_2CuF_4 has been found[13] to be consistent with a KT-type transition slightly modified by 3D interactions. Furthermore, low-q spin waves in K_2CuF_4 (Ref. 14), $BaNi_2(PO_4)_2$, and $BaCo_2(AsO_4)_2$ (Ref. 15) reflect the jump in the spin stiffness constant at T_{KT} predicted by theory,[8,16] and there is some indication[15] of the unbinding of vortices above T_{KT} reflected in the quasielastic neutron scattering of $BaCo_2(AsO_4)_2$.

Measurements of the magnetic susceptibility[17–21] and specific heat[18,22,23] of $NiCl_2$- and $CoCl_2$-GIC's have suggested a two-step ordering process for each with transition temperatures T_l and T_u of 8.0 and 9.1 K for

$CoCl_2$-GIC and 18.1 and 21.3 K for $NiCl_2$-GIC. Both of the pristine compounds $CoCl_2$ and $NiCl_2$ are themselves layered compounds, which exhibit antiferromagnetic (AF) ordering between the spins in adjacent layers.[24,25] It has been suggested[26,27] that the low-temperature phases ($T < T_l$) of $CoCl_2$- and $NiCl_2$-GIC's are likewise phases of long-range AF order along the c axis, and that the intermediate-temperature region ($T_l < T < T_u$) might correspond to the 2D bound vortex phase. While preliminary neutron scattering[26,28] has found AF interplanar correlations below T_l for stage-2 $CoCl_2$-GIC, the need has arisen for a more detailed study to elucidate the nature of the two-step ordering. In this paper we present the results of such a study by elastic neutron scattering, which follows as an elaboration of our earlier work.[29,30]

II. PHYSICAL PROPERTIES OF MCl_2-GIC's

A. Crystal structure

The intercalate layer of MCl_2-GIC (where M=Co or Ni) consists of a three-layer sandwich of Cl-M-Cl layers with approximately the same layered structure as the pristine metal chloride MCl_2 (see Fig. 1).[24,25] The c-axis repeat distance for the stage-2 graphite intercalation compounds is measured by neutron diffraction to be 12.70 Å for $CoCl_2$-GIC and 12.78 Å for $NiCl_2$-GIC, with the distance between successive graphite layers approximately the same as in pristine graphite, 3.35 Å.

The intercalate layers form triangular lattices which are translationally incommensurate with the graphite host, but are rotationally locked with respect to it. Electron-diffraction patterns have shown that the a axis of the intercalate layer is rotated with respect to the graphite a axis by an angle of 30° in $CoCl_2$-GIC (Ref. 26) and by 0° in $NiCl_2$-GIC.[31] Intercalation appears not to change the in-plane lattice parameters of either the intercalant or the graphite substantially. We have measured the lattice constants of stage-2 $CoCl_2$-GIC and $NiCl_2$-GIC to be 3.56±0.01 and 3.46±0.01 Å, respectively, versus 3.553 (Ref. 24) and 3.465 Å (Ref. 25) in the pristine metal chlorides.

The intercalate layers have been found to break up into small domains or islands of roughly 100–200 Å diameter. Much previous work has focused on the role of Cl_2 or complexing halides in the intercalation process. It is thought[31,32] that excess chlorine accumulates along the perimeter of each island and provides sites for charge transfer between the intercalate and graphite layers. Small-angle scattering and diffraction-linewidth measurements[33] have suggested 150-Å islands in $NiCl_2$-GIC. The $CoCl_2$-GIC islands have been reported as 150–170 Å in diameter,[34] or as ellipsoids of mean dimensions 100×500 Å^2.[27]

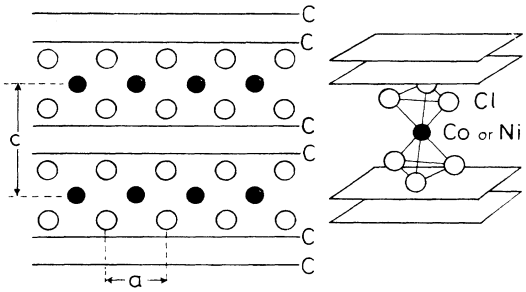

FIG. 1. The crystal structure of stage-2 MCl_2-GIC (M=Co or Ni). Metal ions are indicated by solid circles, Cl by open circles, and graphite layers by solid lines. The c and a axes are as shown in the left-hand panel.

Since the MCl_2 and graphite sublattices are incommensurate, diffraction scans can be indexed relative to the in-plane axes of either sublattice. In this paper we will adopt the notation of specifying an index relative to the metal chloride by a "Co" or "Ni" before the Miller indices (h,k,l), and one relative to the graphite host by a "G."

B. Magnetic structure

Magnetism in $CoCl_2$- and $NiCl_2$-GIC's is presumed to originate from localized moments on the metal ions within the intercalate layers. We assume that their magnetic behavior is analogous to that of the pristine metal chlorides, discussed in detail by Lines.[35] Free ions of Co^{2+} and Ni^{2+} have spin and orbital angular momentum (S,L) of $(\frac{3}{2},3)$ and (1,3), respectively. The combined effect of the crystal field and spin-orbit coupling within these compounds quenches the orbital momentum of $NiCl_2$-GIC and, for $CoCl_2$-GIC, leads to a ground-state Kramers doublet which can be mapped onto a system with $L=0$, $S=\frac{1}{2}$. The spin Hamiltonian appropriate for $CoCl_2$-GIC can be written in terms of the fictitious spins of magnitude $\frac{1}{2}$ as[36]

$$\mathcal{H} = -2J \sum_{\langle i,j \rangle} \mathbf{S}_i \cdot \mathbf{S}_j + 2J_A \sum_{\langle i,j \rangle} S_i^z S_j^z + 2J' \sum_{\langle i,m \rangle} \mathbf{S}_i \cdot \mathbf{S}_m \ , \tag{4}$$

where the first two sums extend over nearest neighbors within the intercalate plane, and the last sum is over nearest neighbors in adjoining layers. The constants J, J', and J_A are the intraplanar, interplanar, and anisotropy exchange interactions, respectively. These exchange constants have been determined by magnetization measurements[36] to be J=7.75 K, $J'/J \approx 8\times10^{-4}$, and J_A/J=0.48. The small interplanar interaction makes $CoCl_2$-GIC a good approximation to a 2D spin system, while the large-anisotropy term leads to pronounced XY behavior.

A slightly different spin Hamiltonian is commonly employed[37–39] in describing $NiCl_2$-GIC:

$$\mathcal{H} = -2J \sum_{\langle i,j \rangle} \mathbf{S}_i \cdot \mathbf{S}_j + D \sum_i (S_i^z)^2 + 2J' \sum_{\langle i,m \rangle} \mathbf{S}_i \cdot \mathbf{S}_m \ , \tag{5}$$

where D is the single-ion anisotropy term. Magnetization measurements yield J=8.75 K (Ref. 20), while the XY anisotropy is much smaller than in $CoCl_2$-GIC, with D probably on the same order as that in pristine $NiCl_2$, 0.80 K.[37] Because of its reduced anisotropy, $NiCl_2$-GIC

is expected to be less likely to exhibit the spin vortex phase than $CoCl_2$-GIC.

III. EXPERIMENT

The samples used in the neutron-diffraction measurements were prepared by vapor reaction of single crystals of Kish graphite with the powdered anhydrous metal chloride in a Cl_2 atmosphere of 740 Torr. Intercalation was continued for 3–6 weeks at 560 °C. Weight-uptake measurements and x-ray diffraction along $(0,0,l)$ were used to check stage fidelity.

In order to obtain large enough samples to collect appreciable intensity, from 20 to 40 of the small Kish-graphite-based samples were arranged together on a thin Al foil. The resulting crystal texture was similar to that of pyrolytic graphite, with random in-plane orientation and a c-axis mosaic spread of about 7°. A somewhat larger sample with a mosaic spread of 10° was employed for the higher-resolution in-plane measurements of $CoCl_2$-GIC.

Most of the neutron-diffraction study was carried out at the Oak Ridge National Laboratory High Flux Isotope Reactor on a triple-axis spectrometer set for zero energy transfer. An incident-neutron wavelength of 2.35 Å was used with a pyrolytic-graphite filter to eliminate higher-order reflections from the monochromator. The $(0,0,l)$ scan of $CoCl_2$-GIC presented in Fig. 2 was taken at Brookhaven National Laboratory on beam line H-4.

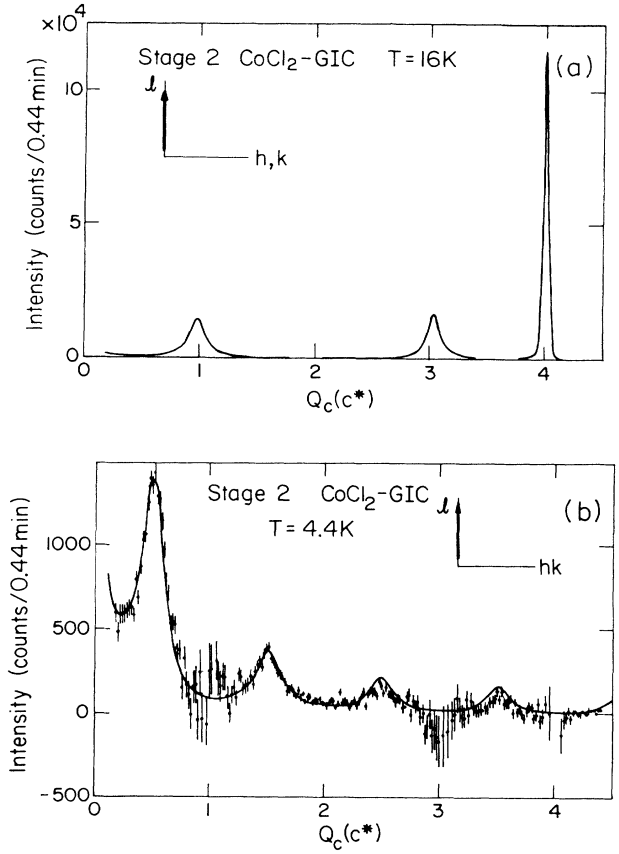

FIG. 2. (a) Nuclear scattering of $CoCl_2$-GIC along $(0,0,l)$. The inset shows the direction of the scan in reciprocal space. On this scale the Hendricks-Teller fit from Eq. (A1) is indistinguishable from the data. (b) Corresponding magnetic scattering at $T=4.4$ K. The solid line is a fit [after Eq. (16)] assuming a stage-dependent spin deviation, as described in the text.

IV. NEUTRON SCATTERING

The coherent elastic scattering cross section for thermal neutrons is directly related to the space Fourier transform of the nuclear and spin-density distributions in the scattering medium. For incident and scattered wave vectors $\mathbf{k}$ and $\mathbf{k}'$, the nuclear scattering function for unpolarized neutrons is[40]

$$S_{\rm nuc}(\mathbf{Q})=\frac{\bar{b}^2}{N}\sum_{i,j} e^{-i\mathbf{Q}\cdot(\mathbf{R}_i-\mathbf{R}_j)} f_{\mathbf{Q}}(\mathbf{R}_i-\mathbf{R}_j)\ , \tag{6}$$

where $\mathbf{Q}=\mathbf{k}-\mathbf{k}'$, $\bar{b}$ is the average scattering length, and

$$f_{\mathbf{Q}}(\mathbf{R}_i-\mathbf{R}_j)=\bar{b}^{-2}\sum_{i,j} b_i b_j \langle \exp[-i\mathbf{Q}\cdot(\mathbf{u}_i-\mathbf{u}_j)]\rangle\ , \tag{7}$$

b_i, $\mathbf{R}_i$, and $\mathbf{u}_i$ being the scattering length, mean atomic position, and deviation at site i.

The magnetic scattering cross section is of similar form,[41]

$$S_{\rm mag}(\mathbf{Q})=[(r_0^2\gamma^2)/N]\,|f(\mathbf{Q})|^2 \times\sum_{i,j} e^{-i\mathbf{Q}\cdot(\mathbf{R}_i-\mathbf{R}_j)} g_\perp(\mathbf{R}_i-\mathbf{R}_j)\ , \tag{8}$$

where $r_0=e^2/mc^2$ is the classical electron radius, γ is the neutron gyromagnetic ratio, $f(\mathbf{Q})$ is the magnetic form factor, and

$$g_\perp(\mathbf{R}_i-\mathbf{R}_j)=\sum_{\alpha,\beta}\left[\delta_{\alpha,\beta}-\frac{Q_\alpha Q_\beta}{Q^2}\right]\langle S_i^\alpha S_j^\beta\rangle\ . \tag{9}$$

The indices α,β run over the Cartesian coordinates, and the Kronecker δ term in Eq. (9) is a selection rule that reflects the fact that the neutron effectively interacts only with the component of the spin which is perpendicular to the scattering vector $\mathbf{Q}$.

The observed intensity depends additionally on the mosaic distribution of crystallites within the sample. Like pyrolytic graphite, the samples used in the present study have random in-plane orientation and a sizable mosaic spread about the c axis. Stephens *et al.*[42] have shown that for longitudinal scans within the plane, the powder-averaged intensity is given by

$$I_p(\mathbf{Q})=\int_0^{\pi/2} d\psi\, P'(\psi) I_c(Q\cos\psi) F(Q\sin\psi)\ , \tag{10}$$

where $I_c(Q)$ is the in-plane component of the scattering function cylindrically averaged about the c axis, $F(Q)$ governs any modulation of $S(\mathbf{Q})$ along the c axis, and $P'(\psi)$ is an effective probability distribution for tipping the crystallite c axis an angle ψ from its average orientation. For a Gaussian rocking curve with full width at half maximum (FWHM) of $2\xi[\ln(2)]^{1/2}$, $P'(\psi)$ is approx-

imately given by

$$P'(\psi)=(\pi^{1/2}/\xi)\exp[-(\psi/\xi)^2](\cos\psi)^{1/2} . \quad (11)$$

Finally, to extract the observed intensity, $I_p(Q)$ must be convoluted with the instrumental resolution function $R(\mathbf{Q})$, which for neutron scattering is a Gaussian ellipsoid.[43] To good approximation, a one-dimensional convolution in the direction of the scan may be used, giving

$$I_{\rm obs}(Q)=\int dq\, I_p(q)R(Q-q) . \quad (12)$$

V. DATA AND ANALYSIS

A. Stage-2 $CoCl_2$-GIC

Figure 2(a) shows a neutron-diffraction scan in the c^* direction taken at $T=16$ K, well above T_u. These data represent purely nuclear scattering, apart from the negligible, nearly flat contribution from paramagnetic scattering. Peaks at (0,0,1), (0,0,3), and (0,0,4) show that the sample is stage 2; however, the (0,0,1) and (0,0,3) peaks are broadened far beyond instrumental resolution, and shifted to lower and higher **Q**, respectively. This phenomenon, which is common among acceptor GIC's, is explained by the existence of staging disorder, in which, instead of stage-2 packets stacked periodically along the c axis throughout each crystal domain, there exist randomly distributed packets of a variable stage number. The diffraction pattern can be calculated analytically after the method of Hendricks and Teller,[44] and the peak widths and positions have been successfully fitted to a model assuming staging disorder, which is discussed in more detail in Sec. VI.

The magnetic scattering along $(0,0,l)$, taken from a subtraction of scans at 4.4 and 16 K, is shown in Fig. 2(b). It appears to be composed of two parts: a broad featureless background that falls off with increasing scattering vector Q and a series of antiferromagnetic (AF) superlattice reflections at $(0,0,\frac{1}{2})$, $(0,0,\frac{3}{2})$, $(0,0,\frac{5}{2})$, and $(0,0,\frac{7}{2})$. The superstructure reflections represent a doubling of the magnetic unit cell along the c axis. Previous authors[26,34] have taken this as evidence of a well-ordered phase below T_l, in which ferromagnetically aligned intercalate sheets order antiferromagnetically along the c axis. However, the peaks are much broader than instrumental resolution and, moreover, have a shape which is more Lorentzian than Gaussian. These features indicate that the reflections are associated with short-range, rather than the long-range, magnetic order.

The second component of the magnetic scattering—the broad background—can be shown to be a magnetic ridge along the c^* axis, by scanning across it perpendicularly. Figure 3 shows an $(h,0,1.85)$ scan across the ridge at a location removed from both Bragg peaks and superstructure reflections. The presence of a nuclear "peak," represented by open circles, away from any Bragg peaks is due to the staging disorder, which builds up intensity along the $(0,0,l)$ ridge. The magnetic scattering, indicated by squares as a difference between scans at $T=4.4$ and 23.0 K, similarly peaks in a ridge

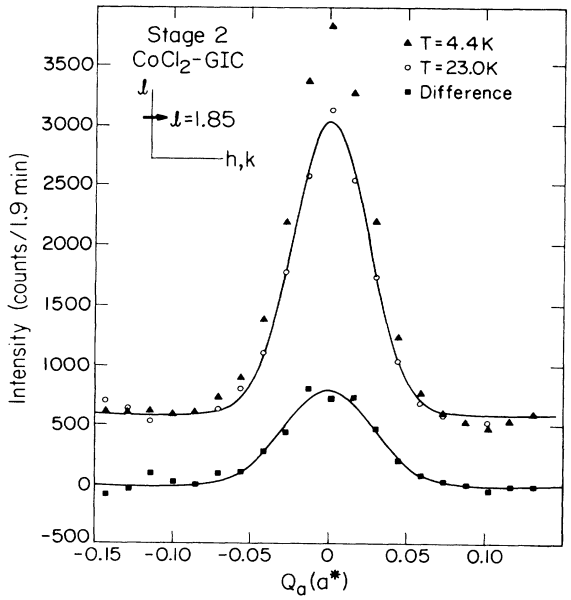

FIG. 3. High- and low-temperature scans across the c^*-axis ridge at $l=1.85$. The inset shows the scan direction. The upper and lower solid lines are Gaussian fits to the nuclear and magnetic scattering at 4.4 K.

along the c^* axis. As we will show in Sec. VI, this magnetic scattering is too strong to be due entirely to staging disorder, and reflects the two dimensionality of the spin-spin correlations. The smooth decrease in intensity of the magnetic ridge and AF reflections with increasing Q in Fig. 2(b) follows $1/Q$, and is due to the dispersion of scattered intensity by the large mosaic spread of the sample.

The temperature dependence of both the magnetic ridge and the AF reflections in the region around $l=\frac{1}{2}$ is shown in Fig. 4(a). As the temperature is raised from 4.4 K both contributions decrease independently, until the $(0,0,\frac{1}{2})$ peak disappears altogether above 8.8 K, which we take as T_l. The integrated intensities of the AF peak, A, and the ridge, B, are shown as a function of temperature in Fig. 4(b). Note that, first, there is a temperature region above T_l in which only 2D spin correlations are present. An abrupt change in the ridge intensity occurs at a higher temperature of 9.5 K, which we interpret as T_u. Second, there is no decrease in ridge intensity below T_l at least as low as 4.4 K, which indicates that the 2D-3D crossover is suppressed, a result consistent with the lack of sharp AF diffraction peaks.

The spin correlation length ξ_c along the c axis is given by $2/\Delta Q_c$, where ΔQ_c is the FWHM of the AF reflection. Figure 4(c) shows ξ_c as a function of temperature. ξ_c grows rapidly below 8.8 K but quickly saturates to a constant value of 22 Å, or less than two magnetic layers. This behavior shows that the spin correlations in $CoCl_2$-GIC are quite two dimensional, even well below T_l.

Information about how the intercalate layers are

translated relative to each other perpendicular to the c axis is obtained by scanning along (h,k,l) with fixed h,k. Figure 5 shows diffraction patterns along Co(1,0,l) and Co(1,1,l). The nuclear scattering for both scans has no sharp features in the region between $l=0$ and 1, which indicates that each $CoCl_2$ layer is translationally uncorrelated with respect to its neighbors. In addition, the

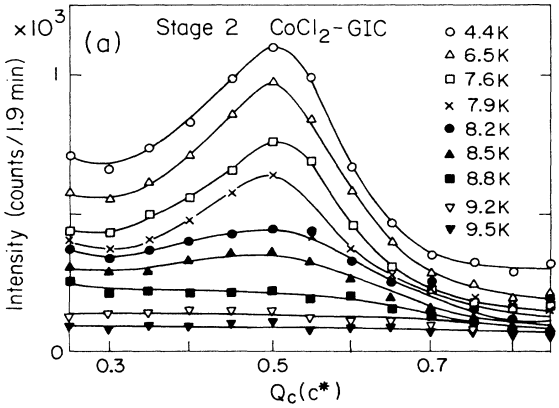

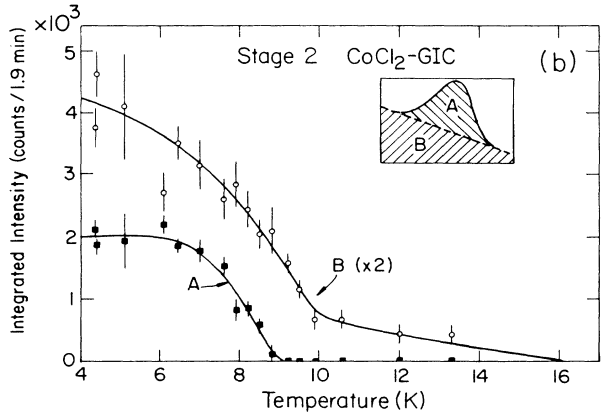

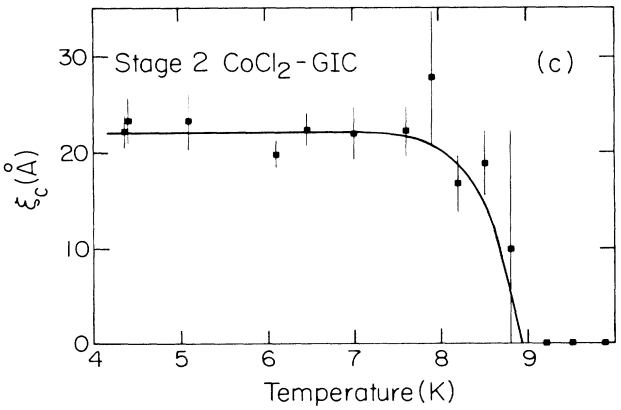

FIG. 4. (a) The magnetic component of scattering along $(0,0,l)$ near the AF $(0,0,\frac{1}{2})$ reflection at various temperatures. (b) Temperature dependence of the intensity integrated under the Lorentzian AF component, A, and under the 2D magnetic ridge, B. (c) Temperature dependence of the spin correlation length along the c axis, taken from the width of the AF peak. The solid lines in all three figures are guides to the eye.

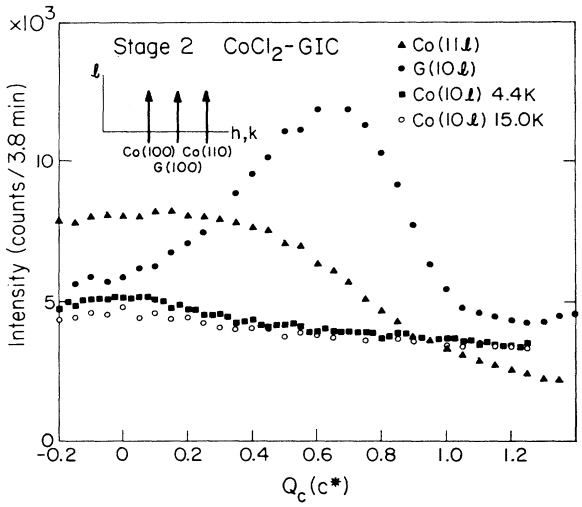

FIG. 5. Fixed h,k scans along the ridges parallel to c^*. The inset shows the scan directions in reciprocal space. Lack of sharp structure indicates lack of translational correlation between layers.

nuclear intensities lie along ridges parallel to c^*, as evidenced by well-defined peaks in the in-plane longitudinal scan at positions corresponding to Co(1,0,0) and Co(1,1,0) (see, for example, Fig. 6). The magnetic component of the scattering along Co(1,0,l), shown implicitly as the difference between low- and high-temperature scans in Fig. 5, likewise occurs as a featureless ridge. The modulation of the ridge of nuclear scattering along Co(1,0,l) and Co(1,1,l) depends on the relative orientations of the Cl and Co atoms in each unit cell. At present, scans do not extend out to high enough Q_c to fit the data conclusively to an interlayer stacking model. However, data are not inconsistent with the atomic arrangement found in pristine $CoCl_2$. The stacking of the graphite layers relative to each other similarly cannot be

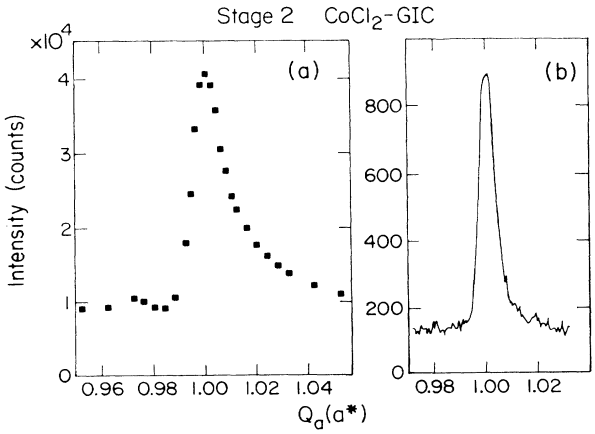

FIG. 6. Longitudinal scans above the ordering temperature through Co(1,0,0) by (a) neutron scattering and (b) x-ray diffraction.

conclusively determined from the observed scattering along G(1,0,l) until more detailed scans are made. Such scans are scheduled shortly.

In order to probe the in-plane magnetic correlations, we have initiated a study of the Co(1,0,0) reflection with improved resolution and counting statistics. Figure 6(a) shows the nuclear scattering profile of the Co(1,0,0) reflection. Two features deserve special note. First, the peak exhibits the characteristic asymmetry of the Warren line shape,[45] which reflects the large mosaic spread and the lack of a well-defined stacking sequence between intercalate layers. Second, the peak is much narrower than would be expected from an average island diameter of 170 Å, as reported by Matsuura *et al.*[34] The peak widths of the G(1,0,0) and the Al(2,0,0) reflections (the latter from the aluminum sample can) are resolution limited with values of 0.022 Å^{-1}. For the present experimental setup, this corresponds[46] to a resolution at Co(1,0,0) of approximately 0.0195 Å^{-1}. Fitting the low-Q side of the reflection, which does not depend strongly on the Warren line shape, gives an intrinsic FWHM of $\Delta Q=0.0090$ Å^{-1} after deconvolution with instrumental resolution. The mean island size L obtains from the Scherrer formula,

$$L=(2\pi/\Delta Q)(4\ln 2/\pi)^{1/2}\ , \tag{13}$$

as $L=650\pm150$ Å, the large uncertainty arising from difficulty in assessing the resolution width. This result lies between the value 440 Å obtained from high-resolution x-ray measurements shown in Fig. 6(b), and a value of roughly 900 Å determined from neutron scattering measurements to appear elsewhere.[47] All three determinations give larger values than reported elsewhere,[27,34] the difference perhaps being due to intercalation conditions.

The magnetic scattering around Co(1,0,0) at 4.4 and 9.2 K, taken from a subtraction of scans at those temperatures and one at 16 K, is shown in Fig. 7. The magnetic reflection at 4.4 K is somewhat narrower than the corresponding nuclear scattering. The difference is likely due to a modulation of the nuclear scattering function along the Co(1,0,l) rod. Assuming the same intralayer stacking as in pristine $CoCl_2$, the modulation has a minimum at $l=0$, making the Warren line-shape asymmetry more pronounced for the nuclear scattering than for the magnetic scattering, which gives essentially flat rods. Such a modulation is not observed directly in the Co(1,0,l) scan because the mosaic serves to disperse the intensity into wider regions of reciprocal space as l increases.

The tails of the magnetic scattering at 4.4 K do not extend very far, and appear to fall off faster than a power law. This suggests that the scattering below T_l obeys a usual Gaussian structure factor, rather than the form predicted for the bound vortex phase. Quantitative fits of the scattering to both structure factors will be presented in Sec. VI. The scattering at $T=9.2$ K, also shown in Fig. 7, is too weak with present counting statistics to discriminate the peak shape accurately.

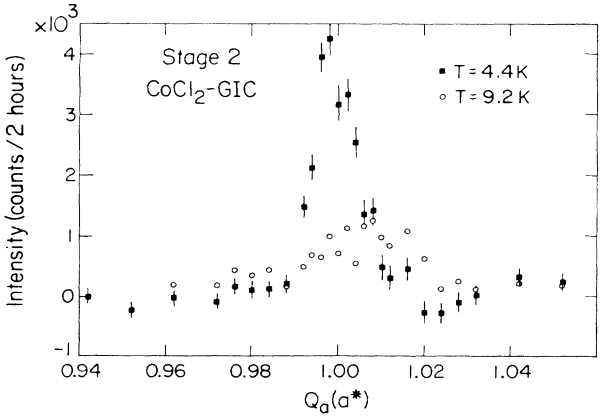

FIG. 7. Magnetic contribution to the intensity around Co(1,0,0) below T_l at 4.4 K and near T_u at 9.2 K.

B. Stage-2 $NiCl_2$-GIC

Figure 8(a) shows the nuclear contribution to scattering along (0,0,l) for $NiCl_2$-GIC, taken well above the or-

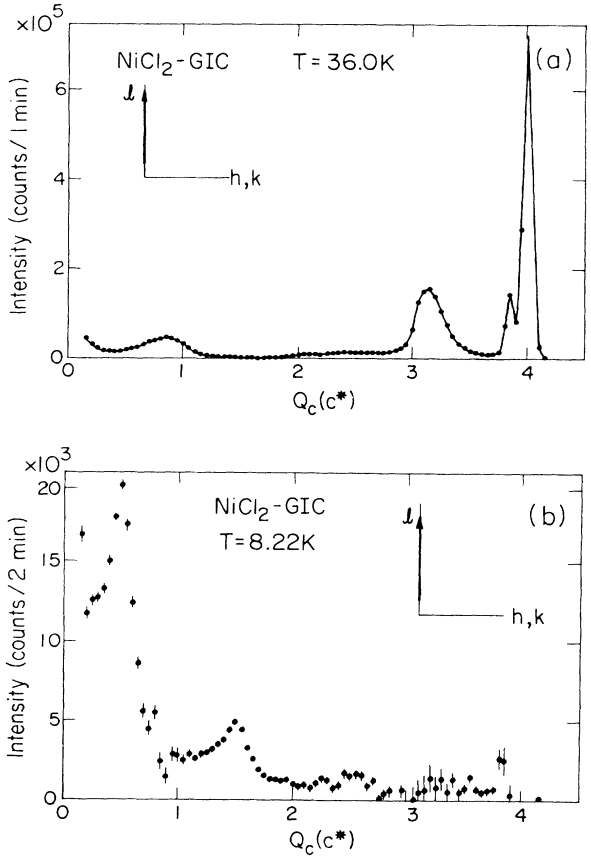

FIG. 8. (a) Nuclear scattering component of an (0,0,l) scan for $NiCl_2$-GIC. The inset shows the scan direction. The peak at $l=3.85$ is due to pristine graphite, and the broadening and shift of the peak positions of the (0,0,1) and (0,0,3) reflections is due to staging disorder, as discussed in the text. (b) Magnetic scattering along (0,0,l) below T_l.

dering temperature at 36 K. The spectrum reveals that the sample is composed of substantial amounts of the stage-3 compound, as well as some pristine graphite. The magnetic contribution below T_l, extracted by subtracting this spectrum from one taken at $T=8.2$ K, appears in Fig. 8(b). AF superstructure reflections appear at $l=\frac{1}{2}$, $\frac{3}{2}$, $\frac{5}{2}$, and $\frac{7}{2}$, superposed on a smooth ridge along $(0,0,l)$, as for $CoCl_2$-GIC. This result is contrasted with an earlier neutron scattering study[33] of a stage-2 $NiCl_2$-GIC powder, which found no magnetic ordering along the c^* axis.

The temperature dependence of the $(0,0,\frac{1}{2})$ reflection was investigated in detail. Figure 9(a) shows the intensity around $(0,0,\frac{1}{2})$ at various temperatures, and the integrated intensities of the magnetic ridge and the Lorentzian AF reflection are plotted versus temperature in Fig. 9(b). These data are strikingly similar to those of $CoCl_2$-GIC, and the c-axis spin correlation length ξ_c of $NiCl_2$-GIC, shown in Fig. 9(c), behaves analogously as well. Taken together, these data reflect a two-stage ordering process for $NiCl_2$-GIC, as for $CoCl_2$-GIC.

A further similarity can be seen in the scans along (h,k,l) with fixed h,k. Figure 10 shows the Ni$(1,0,l)$, Ni$(1,1,l)$, and G$(1,0,l)$ scans from $l=0$ to 1.2. Once again the observed intensity lies in ridges parallel to the c^* axis, and no fine structure is present between $l=0$ and 1, showing that the $NiCl_2$ layers are translationally uncorrelated. The difference in details of the scattering intensity is attributable to the orientation of the Cl layers relative to the metal sublattice. Further scans out to higher values of l that are required to determine the intralayer stacking of the intercalate and the graphite layers are planned to begin shortly.

VI. DISCUSSION

A. $CoCl_2$-GIC

1. *Interplanar reflections*

In order to understand the nature of the interplanar magnetic interactions, it is essential to identify and decouple the effects that lead to the broadening of the AF reflections at $(0,0,\frac{1}{2})$, $(0,0,\frac{3}{2})$, ... Broadening can be the result of either spin disorder or spatial disorder of the atoms on which the spins lie. The latter condition is present in $CoCl_2$-GIC, as evidenced from the Hendricks-Teller (HT) broadening of the nuclear $(0,0,l)$ reflections. To see whether staging disorder alone can account for the magnetic scattering profile, we have fitted the nuclear scattering to a HT model,[44] which is discussed in detail in Appendix A.

A fit of the nuclear peak positions and widths of $CoCl_2$-GIC yields the following mixture of stages: 5.5% stage 1, 70% stage 2, 14% stage 3, 8% stage 4, and 2.5% stage 5. On the scale of Fig. 2(a), the fit and data are indistinguishable. If such a sample were to align with AF long-range order along the c axis, the structural disorder would selectively broaden the AF reflections as it did the nuclear reflections. For the five types of nuclear layers present in the sample, there are 25 types of antiferromagnetic packets, due to the doubling of the average magnetic unit cell. The scattering along $(0,0,l)$ from such a sample with the nuclear stage fractions given above is shown in Fig. 11, where the theoretical plot from Eq. (A1) has been multiplied by $1/Q$ and by $|f(Q)|^2$ (Ref. 48) for direct comparison with the exper-

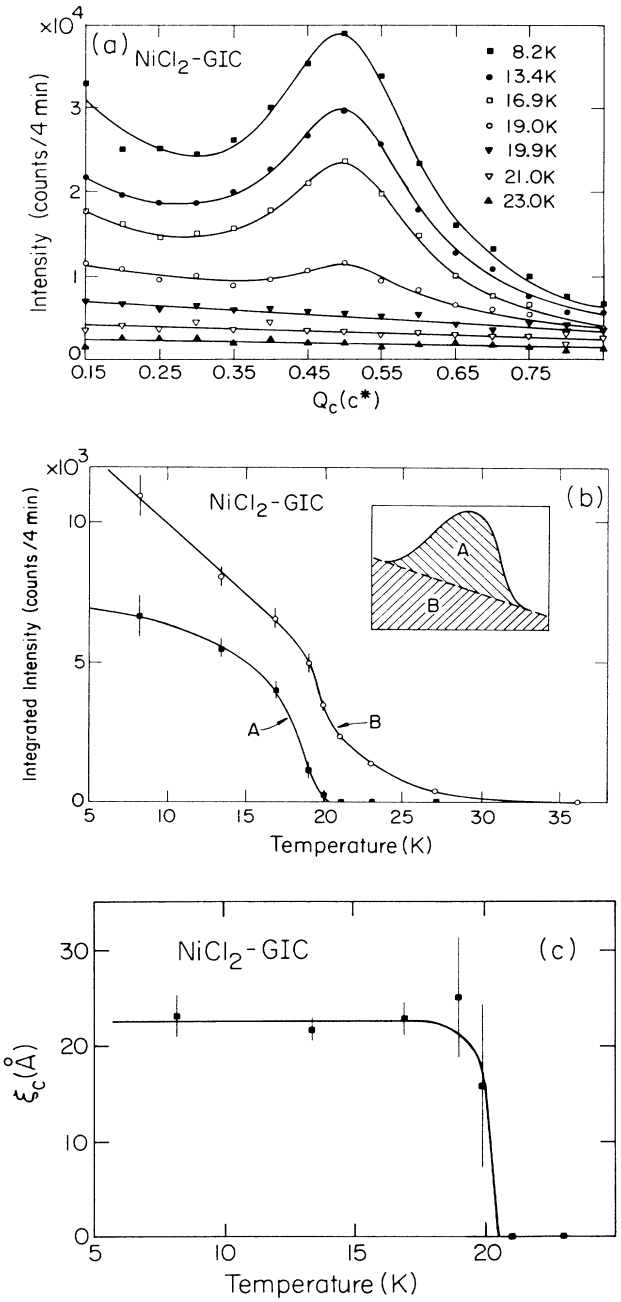

FIG. 9. (a) The magnetic component of scattering along $(0,0,l)$ near the AF $(0,0,\frac{1}{2})$ reflection at various temperatures. (b) Temperature dependence of the intensity integrated under the Lorentzian AF component, A, and under the 2D magnetic ridge, B. (c) Temperature dependence of the spin correlation length along the c axis, taken from the width of the AF peak. The lines in all three figures are guides for the eye.

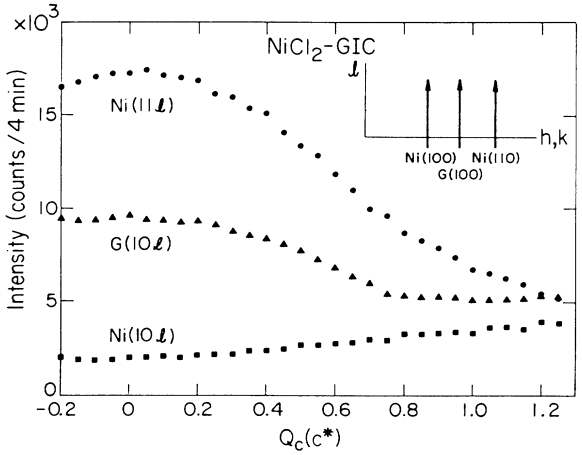

FIG. 10. Fixed h,k scans for $NiCl_2$-GIC. Inset shows the directions of the scans in reciprocal space.

imental data. Smoothed data from Fig. 2(b) are overlayed as a dashed line in Fig. 11. The fit is quite poor on two counts: First, the theoretical peak widths are too narrow, indicating the presence of spin disorder. Second, the HT model predicts a shift of the peak positions away from $l=\frac{1}{2},\frac{3}{2},\frac{5}{2},\ldots$, which is more pronounced than the data indicate. As we will show below, this feature indicates that the spin disorder must have some dependence on the number of carbon layers intervening between the spins.

To investigate the effects of spin disorder we assume the following model for classical XY spins, in which the

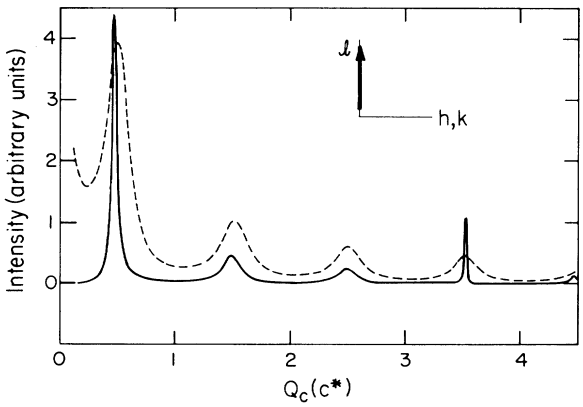

FIG. 11. The solid line represents a simulation of the magnetic scattering along $(0,0,l)$ that would result from AF long-range order in $CoCl_2$-GIC, based on the Hendricks-Teller model (Ref. 44). The intensity has been multiplied by $|f(Q)|^2/Q$ for direct comparison to experimental data in Fig. 2(b), which are reproduced in this figure by a dashed line. The agreement is quite poor in two respects. First, the observed broadening of the reflections over that predicted by the HT model is indicative of spin disorder. Second, the shift of peak positions away from $l=\frac{1}{2},\frac{3}{2},\frac{5}{2},\ldots$, is not as pronounced as predicted by the model, which suggests that the spin disorder grows with increasing stage number.

total spin in a given intercalate layer is not exactly antiparallel to that in an adjacent layer, but deviates somewhat by a rotation in the intercalate plane. We shall initially assume that the total spin in each layer is constant and that the layers are equally spaced with spacing c. Later we will relax these constraints.

Let ϕ_n be the orientation of the total spin S in the nth intercalate layer relative to an arbitrary x axis. Since the spins are constrained to the intercalate plane, the diffracted intensity in a scan along the c^* axis is proportional to I_Q, given by

$$I_Q \equiv \langle \mathbf{S}(Q)\cdot\mathbf{S}(-Q)\rangle \ , \tag{14}$$

where $\mathbf{S}(Q)$ is the Fourier-transformed spin. The expression above is evaluated for the case of a disordered antiferromagnet in Appendix B. For a sufficiently large lattice the intensity is approximately given by

$$I_Q \approx S^2N\left[1-\frac{x_Q}{1+x_Q}-\frac{x_{-Q}}{1+x_{-Q}}\right] , \tag{15}$$

where $x_Q \equiv \langle\cos\Delta\phi\rangle e^{iQc}$ and where $\Delta\phi$ is the deviation of the spin orientation in one intercalate layer from AF alignment with the preceding one. I_Q peaks at odd multiples of π/c, as expected.

Before applying this result to the case of $CoCl_2$-GIC we must include two other effects. First, since there is a considerable variation in the size of the intercalate islands,[27] there is no guarantee that the total spin in each layer is the same. Let the magnitude of the total spin in the jth intercalate layer be written as $S_j=\langle S\rangle+\Delta S_j$, where $\langle\Delta S_j\rangle=0$. Assuming that the S_j can vary independently of each other and of their orientations, ϕ_j, then the net effect of the spin variation is to change S^2 in Eq. (15) to $\langle S\rangle^2$, and to add a constant term due to self-correlation, $(\langle S^2\rangle-\langle S\rangle^2)N$.

The second effect to be considered is a relaxation of the constraint of equally spaced lattice points, an essential modification in light of the staging disorder. An analysis parallel to the one above gives an identical result with the phase term e^{iQc} replaced by a sum over the possible phases weighted by their probabilities of occurring. If we further suppose that $\Delta\phi_n$ depends on the lattice spacing c_n, then for large crystals, Eq. (15) becomes

$$I_Q=\langle S\rangle^2N\left[1-\frac{y_Q}{1+y_Q}-\frac{y_{-Q}}{1+y_{-Q}}\right]+(\langle S^2\rangle-\langle S\rangle^2)N \ . \tag{16}$$

The quantity y_Q is defined in analogy to x_Q as

$$y_Q \equiv \sum_t f^{(t)}\langle\cos\Delta\phi^{(t)}\rangle e^{iQc^{(t)}} \ , \tag{17}$$

where $f^{(t)}$ and $c^{(t)}$ are the fraction and lattice spacing of the tth-stage intercalate layer, obtained above, and $\Delta\phi^{(t)}$ is the spin deviation, which now depends on stage number. Equation (17) states that the weighting factor of the phase of a particular stage layer depends not only on the fraction of that stage present, but on the degree of spin alignment as well.

Equation (16) leads to unsatisfactory fits of the magnetic scattering along $(0,0,l)$ if $\langle \cos\Delta\phi^{(t)} \rangle$ is required to be independent of stage t. This can be seen by comparing peak positions in Figs. 2(a) and 2(b). Whereas nuclear (0,0,1) and (0,0,3) peaks are shifted toward the stage-3 (0,0,1) and (0,0,4) peak positions, respectively, the magnetic peaks are not shifted at all. [This effect is even more prominent for $NiCl_2$-GIC. See Figs. 8(a) and 8(b).] This indicates that AF alignment is most complete at lower stages, as this condition would give the greater weight in Eq. (17) to the peak positions of the lower stage layers. The solid line in Fig. 2(b) is a fit with $\langle \cos\Delta\phi^{(1)} \rangle \approx 1$, $\langle \cos\Delta\phi^{(2)} \rangle = 0.65$, and $\langle \cos\Delta\phi^{(t)} \rangle = 0$ for $t \geq 3$. The small discrepancy in intensities at $(0,0,\frac{5}{2})$ and $(0,0,\frac{7}{2})$ is likely on account of the large vertical mosaic spread, which at higher angles adds a $1/Q^2$ component to the fraction of intensity reaching the detector.[49]

2. *Intraplanar reflections*

We now turn our attention to the intraplanar magnetic correlation, as probed by the longitudinal scan through Co(1,0,0). Determination of the peak shape is crucial in ascertaining the form of the spin correlation function. For scattering vectors perpendicular to the c axis, the magnetic scattering selection rule in Eq. (9) for XY spins is unity, giving a scattering cross section of the form

$$S_{\rm mag}(\mathbf{Q}) \propto (1/N) \sum_{i,j} \exp[-i\mathbf{Q}\cdot(\mathbf{R}_i - \mathbf{R}_j)] \times g(|\mathbf{R}_i - \mathbf{R}_j|) , \quad (18)$$

where $g(R_{ij}) = \langle \mathbf{S}_i \cdot \mathbf{S}_j \rangle$. Moving to the continuum limit and performing the angular integration yields

$$S_{\rm mag}(\mathbf{Q}) \propto \int_0^\infty dR\, J_0(qR) R g(R) , \quad (19)$$

where $q = |\mathbf{Q} - \mathbf{G}|$ for in-plane reciprocal-lattice points $\mathbf{G}$. Dutta and Sinha[50] have shown that the effect on this expression of a distribution of finite islands is to add an additional Gaussian term in the integral to damp off contributions from large R,

$$S_{\rm mag}(\mathbf{Q}) = \tfrac{1}{2}(r_0\gamma)^2 |f(\mathbf{Q})|^2 \frac{2\pi N}{L^2} \times \int_0^\infty dR\, J_0(qR) R g(R) e^{-\pi R^2/L^2} , \quad (20)$$

where L is the mean island diameter.

We shall consider several cases of Eq. (20). Conventional long-range order gives a constant spin correlation function, which leads to a Gaussian scattering profile. Short-range order typically has an exponential form, $g(r) \sim r^{-\eta} \exp(-\xi r)$. For $\xi \ll L$, the finite-size effects can be safely ignored, and the scattering function is of the approximate form of a Lorentzian raised to some power which depends on the value of η and on the effective dimensionality of the correlations. Quasi-long-range order is characterized by a power-law decay of the correlation function, $g(r) \sim r^{-\eta}$. Putting this into Eq. (20) yields

$$S_{\rm mag}(\mathbf{Q}) \propto \Phi(1 - \eta/2; 1; -q^2 L^2/4\pi) ,$$

where Φ is a degenerate hypergeometric function known as Kummer's function.[50]

Each of the scattering functions above has been appropriately powder averaged for a c-axis mosaic spread of 10.0° as per Eq. (10), convoluted with an instrumental resolution of 0.0195 Å^{-1}, and compared with the data. Each fit has three free parameters: a maximum intensity, a flat background which may be nonzero because of paramagnetic scattering at 16 K, and an intrinsic length scale, either L or ξ. Considerations of total spin scattering limit the paramagnetic background to about 50 counts, while the length scales must be consistent with the island size determined from the nuclear Co(1,0,0) reflection. For the Kummer function η is taken as 0.12, the value expected from linear scaling with temperature.

Best fits of the Kummer-function– and Gaussian-based profiles are shown in Fig. 12. For each, $L = 800$ Å, which is the largest allowed island size. The Gaussian function fits marginally better, the only significant difference being in the low-Q tail, which is shown in more detail in the inset. However, the Kummer-function fit is not enough in error to be discounted. For all values of $\xi < 800$ Å, the short-range order function was found to yield unacceptably broad peaks.

While the finite size of the intercalate islands is partially responsible for obscuring the form of $g(r)$, it may be a crucial element in the two-stage ordering that $CoCl_2$-GIC undergoes. Earlier neutron scattering[26] and susceptibility[36] experiments have determined the intraplanar exchange coupling J' to be only a small fraction of the intraplanar coupling J. As the in-plane correlation length ξ_a grows, the effective coupling between layers goes like

$$J'_{\rm eff} \sim (\xi_a/a)^2 J' , \quad (21)$$

where a is the in-plane lattice parameter. If ξ_a were to grow in infinity, $J'_{\rm eff}$ would also diverge, and the 2D and 3D ordering would occur simultaneously. However, in the case of $CoCl_2$-GIC, ξ_a is constrained by the island size, allowing the 2D ordering to occur before $J'_{\rm eff}$ is large enough to bring about 3D order. This mechanism may be additionally responsible for the failure of $CoCl_2$-GIC to achieve 3D long-range magnetic order.

B. $NiCl_2$-GIC

Figure 8(a) shows that the $NiCl_2$-GIC sample has a number of domains which are predominantly stage 3 rather than stage 2, and regions of pristine graphite as well. Because the layers are not randomly mixed throughout the sample, the Hendricks-Teller model no longer applies in its simple form, making a thorough analysis parallel to that of $CoCl_2$-GIC less tractable.

However, a detailed analysis is probably superfluous, in light of the similarity between the magnetic ordering of $NiCl_2$-GIC and $CoCl_2$-GIC in nearly all respects.

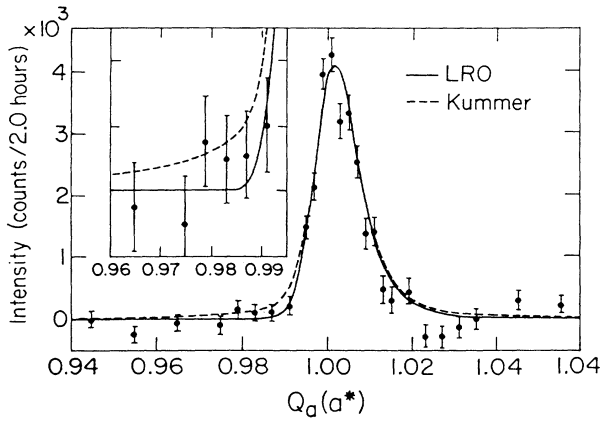

FIG. 12. Fits of the Kummer-function– and Gaussian-based line shapes to Co(1,0,0) data at 4.4 K, following Eq. (20). The Kummer fit has been made with $\eta=0.12$. Both fits represent a cylindrical average of the structure factor based on a mean island size of 800 Å, and both have been corrected for a 10° c-axis mosaic spread and convoluted with an instrumental resolution of 0.0195 Å^{-1}. The inset shows in more detail the low-Q tail where the difference in fits is the greatest.

One exception to this lies in the ratio of the ridge intensity to the AF peak intensity, which is larger by nearly a factor of 2 for $NiCl_2$-GIC than for $CoCl_2$-GIC. This indicates that the two dimensionality of spin correlations is more pronounced in $NiCl_2$-GIC than in $CoCl_2$-GIC, perhaps because of the predominance of high-stage faults along the c axis.

VII. CONCLUSION

The magnetic behavior of stage-2 $CoCl_2$- and $NiCl_2$-GIC is quite similar. Both compounds undergo a two-step ordering. Above T_u the compounds are paramagnetic. For $T_l<T<T_u$ the compounds exhibit only intraplanar ferromagnetic spin correlations with no correlations between different intercalate planes. Below T_l different intercalate sheets are coupled antiferromagnetically by a weak stage-dependent correlation which, as the temperature is decreased, is never observed to lead to long-range magnetic order along the c axis.

In both compounds the structure is quasi-2D, with no well-defined stacking sequence between consecutive intercalate layers. Instead of Bragg points, structural Bragg ridges are present, running parallel to the c^* axis from each of the reciprocal-lattice points in the $(h,k,0)$ plane. Further evidence for these ridges is found in the Warren line shape of the in-plane peaks.

A longitudinal scan through the Co(1,0,0) reflection suggests that the bound vortex state may not exist for $CoCl_2$-GIC below T_l, since the peak shape fits somewhat more successfully to a conventional Gaussian profile than to a cusp shape modified by mosaic spread and finite-size effects. Of greater interest is the peak shape near T_u, which is thought to correspond to T_{KT}. Unfortunately, the counting statistics for the present study were not sufficient to discriminate the peak shape for scattering in the intermediate-temperature regime. However, the existence of finite-sized islands of diameter much larger than previously expected makes it likely that the bound vortex phase is realized between T_l and T_u.

ACKNOWLEDGMENTS

The authors wish to thank S. M. Shapiro for assistance with the measurements at Brookhaven National Laboratory, and R. M. Nicklow and M. E. Hagens for those performed at Oak Ridge. We are also grateful to S. C. Moss, S. K. Sinha, D. A. Neumann, and P. F. Miceli for many fruitful discussions. This work was supported by the National Science Foundation under Grant No. DMR-86-05565.

APPENDIX A

This appendix deals with a model of staging disorder first presented by Hendricks and Teller (HT).[44] According to this model the intensity of a system of random layers t with probability of occurring $f^{(t)}$ is given as

$$I_{\rm av}=\sum_t f^{(t)}|V^{(t)}|^2+2\sum_{s,t} f^{(s)}f^{(t)}|V^{(s)}||V^{(t)}|\left[\frac{\cos(\varphi^{(s)}+\varphi^{(t)}+\alpha^{(s)}+\alpha^{(t)})-C\cos(\varphi^{(s)}+\varphi^{(t)}-\bar{\varphi}+\alpha^{(s)}+\alpha^{(t)})}{1-2C\cos\bar{\varphi}+C^2}\right], \tag{A1}$$

where

$$C\equiv\sum_s f^{(s)}\cos(2\varphi^{(s)}-\bar{\varphi}), \tag{A2}$$

and $\bar{\varphi}$ is defined implicitly by the relation

$$\sum_s f^{(s)}\sin(2\varphi^{(s)}-\bar{\varphi})=0. \tag{A3}$$

The quantity $\varphi^{(s)}$ is half the phase gained across the sth layer, given by $2\varphi^{(s)}=Qc^{(s)}$, where $c^{(s)}$ is the lattice spacing of the layer. Finally, $\alpha^{(s)}$ is the phase of the layer form factor, $V^{(s)}=|V^{(s)}|\exp(i\alpha^{(s)})$.

For $CoCl_2$-GIC the lattice constant for a stage-N packet is roughly

$$c^{(N)}=\begin{cases}9.30\ \text{Å}, & N=1\\ 9.35\ \text{Å}+(N-1)d_C, & N\geq 2\end{cases} \tag{A4}$$

where $d_C=3.35$ Å is the spacing between graphite layers. The distance between Co and Cl layers is taken to be $d_I=1.447$ Å, the value in pristine $CoCl_2$.[24] The layer

form factor can thus be written as

$$V^{(N)}(Q)=B_{\mathrm{Co}}\cos(Q\tfrac{1}{2}c^{(N)}) +2B_{\mathrm{Cl}}\cos[Q(\tfrac{1}{2}c^{(N)}-d_I)]+V_{\mathrm{C}}^{(N)}(Q)\ , \quad \text{(A5)}$$

where

$$V_{\mathrm{C}}^{(N)}(Q)=\begin{cases} B_{\mathrm{C}}\left[1+2\sum_{j=1}^{(N-1)/2}\cos(jd_cQ)\right] & (N \text{ odd})\ , \\ 2B_{\mathrm{C}}\sum_{j=1}^{N/2}\cos\left[\dfrac{2j-1}{2}d_cQ\right] & (N \text{ even})\ . \end{cases} \quad \text{(A6)}$$

The effective scattering lengths per layer B_i are given by the assumed form for the chemical formula of stage-2 $CoCl_2$-GIC, determined by weight uptake and considerations of the island size, $CoCl_{2.03}C_{10.9}$. Assuming the same packing fraction in all stages and that coherence is maintained between graphite layers across gaps in the intercalate, then

$$B_{\mathrm{Co}}=b_{\mathrm{Co}},\quad B_{\mathrm{Cl}}=\frac{2.09}{2}b_{\mathrm{Cl}},\quad B_{\mathrm{C}}=\frac{10.9}{2}b_{\mathrm{C}}\ , \quad \text{(A7)}$$

where the atomic scattering lengths are[51] $b_{\mathrm{Co}}=0.25$, $b_{\mathrm{Cl}}=0.96$, and $b_{\mathrm{C}}=0.664$ (all $\times 10^{-12}$ cm). A smaller value of B_{C} would result if we assumed coherence was maintained only across the intercalate islands. However, if only the peak positions and widths are fitted with no attempt to fit the intensities, then the results are not sensitive to such a change. A fit of the nuclear peak positions and widths of $CoCl_2$-GIC yields the following mixture of stages: 5.5% stage 1, 70% stage 2, 14% stage 3, 8% stage 4, and 2.5% stage 5. On the scale of Fig. 2(a), the fit and data are indistinguishable.

APPENDIX B

We seek to evaluate the expression

$$I_Q\equiv\langle \mathbf{S}(Q)\cdot\mathbf{S}(-Q)\rangle \quad \text{(B1)}$$

for a disordered 1D planar antiferromagnet. Suppose ϕ_n is the orientation of the total spin S in the nth intercalate layer relative to an arbitrary x axis. Then the total spin of the nth layer can be written as

$$\mathbf{S}_n=S(\hat{\mathbf{x}}\cos\phi_n+\hat{\mathbf{y}}\sin\phi_n)\ . \quad \text{(B2)}$$

The Fourier transform of this over all N intercalate layers is

$$\mathbf{S}(Q)=S\sum_{n=0}^{N-1}(\cos\phi_n\hat{\mathbf{x}}+\sin\phi_n\hat{\mathbf{y}})e^{iQnc}\ , \quad \text{(B3)}$$

where $Q=2\pi l/c$. The expression for I_Q thus can be written as

$$I_Q=S^2\sum_{n=0}^{N-1}\sum_{m=0}^{N-1}\langle\cos(\phi_n-\phi_m)\rangle e^{iQc(n-m)}\ . \quad \text{(B4)}$$

For a disordered antiferromagnet,

$$\phi_n=\phi_{n-1}+\pi+\Delta\phi_n,\quad (n=1,2,\ldots,N-1)\ , \quad \text{(B5)}$$

where $\langle\Delta\phi_n\rangle=0$ for all n. Inserting this into Eq. (B4) gives

$$I_Q=S^2\sum_{m=0}^{N-1}\left[1+2\sum_{n=m+1}^{N-1}\langle\cos(\Delta\phi_{m+1}+\Delta\phi_{m+2}+\cdots+\Delta\phi_n)\rangle(-1)^{n-m}\cos[Qc(n-m)]\right]\ . \quad \text{(B6)}$$

Since positive and negative rotations are equally likely, $\langle\sin\Delta\phi_n\rangle$ vanishes for all n. Expansion of the term in angular brackets in Eq. (B6) thus leaves only

$$\langle(\cos\Delta\phi_{m+1})(\cos\Delta\phi_{m+2})\cdots(\cos\Delta\phi_n)\rangle\ .$$

The averaging can be done separately over each layer, and the expression reduces to $\langle\cos\Delta\phi\rangle^{n-m}$, where we have eliminated the unnecessary subscript on $\Delta\phi$. Equation (B6) becomes

$$I_Q=S^2\sum_{m=0}^{N-1}\left[1+\sum_{k=1}^{N-m-1}[(-x_Q)^k+(-x_{-Q})^k]\right]\ , \quad \text{(B7)}$$

where $x_Q\equiv\langle\cos\Delta\phi\rangle e^{iQc}$. The sum over k can be evaluated in the usual way, using the relation

$$\sum_{j=1}^{R}x^j=x\left[\frac{1-x^R}{1-x}\right]\ . \quad \text{(B8)}$$

Upon simplifying the summing over the index m we obtain

$$I_Q=S^2N\left[1-\frac{x_Q}{1+x_Q}-\frac{x_{-Q}}{1+x_{-Q}}\right] +S^2\left[\frac{x_Q}{1+x_Q}\left[\frac{1-(-x_Q)^N}{1+x_Q}\right] +\frac{x_{-Q}}{1+x_{-Q}}\left[\frac{1-(-x_{-Q})^N}{1+x_{-Q}}\right]\right]\ . \quad \text{(B9)}$$

The first term overwhelms the second whenever

$$1-\langle\cos\Delta\phi\rangle\gg 1/N\ ;$$

that is, for either large or very disordered spin systems. This condition holds for $CoCl_2$-GIC, and the expression for I_Q reduces to

$$I_Q\approx S^2N\left[\frac{1-\langle\cos\Delta\phi\rangle^2}{1+\langle\cos\Delta\phi\rangle^2+2\langle\cos\Delta\phi\rangle\cos(Qc)}\right]\ , \quad \text{(B10)}$$

which peaks at odd multiples of π/c. The corresponding FWHM is

$$\Delta Q=\frac{2}{c}\cos^{-1}\left[1-\frac{(1-\langle\cos\Delta\phi\rangle)^2}{2\langle\cos\Delta\phi\rangle}\right]\ . \quad \text{(B11)}$$

*Present address: Department of Physics, State University of New York at Binghamton, Binghamton, NY 13901.

[1]M. S. Dresselhaus, in *Festkörperprobleme Advances in Solid State Physics,* edited by P. Grosse (Vieweg, Braunschweig, 1985), Vol. 25, p. 21.

[2]M. S. Dresselhaus, Phys. Today **37(3)**, 60 (1984).

[3]H. Zabel and P. C. Chow, Comm. Cond. Mat. Phys. **12**, 225 (1986).

[4]M. Matsuura, Ann. Phys. (Paris) Colloq. **11**, C2-117 (1986).

[5]J. M. Kosterlitz and D. J. Thouless, J. Phys. C **6**, 1181 (1973).

[6]J. M. Kosterlitz, J. Phys. C **7**, 1046 (1974).

[7]J. V. José, L. P. Kadanoff, S. Kirkpatrick, and D. R. Nelson, Phys. Rev. B **16**, 1217 (1977).

[8]D. L. Huber, Phys. Rev. B **26**, 3758 (1982).

[9]N. D. Mermin and H. Wagner, Phys. Rev. Lett. **17**, 1133 (1966); N. D. Mermin, Phys. Rev. **176**, 250 (1968).

[10]D. E. Moncton, R. Pindak, S. C. Davey, and G. S. Brown, Phys. Rev. Lett. **49**, 1865 (1982); S. C. Davey, J. Budai, J. W. Goodby, R. Pindak, and D. E. Moncton, *ibid.* **53**, 2129 (1985).

[11]D. J. Bishop and J. D. Reppy, Phys. Rev. B **22**, 5171 (1980); D. McQueeney, G. Agnolet, and J. D. Reppy, Phys. Rev. Lett. **52**, 1325 (1984).

[12]D. J. Resnick, J. C. Garland, J. T. Boyd, S. Shoemaker, and R. S. Newrock, Phys. Rev. Lett. **47**, 1542 (1981); R. A. Webb, R. F. Voss, G. Grinstein, and P. M. Horn, *ibid.* **51**, 690 (1983).

[13]K. Hirakawa, H. Yoshizawa, and K. Ubukoshi, J. Phys. Soc. Jpn. **51**, 2151 (1982).

[14]K. Hirakawa, H. Yoshizawa, J. D. Axe, and G. Shirane, J. Phys. Soc. Jpn. **52**, 4220 (1983).

[15]L. P. Regnault, J. Rossat-Mignod, J. Y. Henry, R. Pynn, and D. Petitgrand, in *Magnetic Excitations and Fluctuations,* Vol. 54 of *Springer Series in Solid State Sciences,* edited by S. W. Lovesey, U. Balucani, F. Borsa, and V. Tognetti (Springer, Berlin, 1984), p. 201; L. P. Regnault, J. P. Boucher, J. Rossat-Mignod, J. Bouillot, R. Pynn, J. Y. Henry, and J. P. Renard, Physica **136B**, 329 (1986).

[16]D. R. Nelson and J. M. Kosterlitz, Phys. Rev. Lett. **39**, 1201 (1977).

[17]Yu. S. Karimov, Zh. Eksp. Teor. Fiz. **66**, 1121 (1974) [Sov. Phys.—JETP **39**, 547 (1974)].

[18]Yu. S. Karimov, Zh. Eksp. Teor. Fiz. **68**, 1539 (1975) [Sov. Phys.—JETP **41**, 772 (1976)].

[19]Y. Murakami, M. Matsuura, M. Suzuki, and H. Ikeda, J. Magn. Magn. Mater. **31-34**, 1171 (1983).

[20]H. Suematsu, R. Nishitani, R. Yoshizaki, M. Suzuki, and H. Ikeda, J. Phys. Soc. Jpn. **52**, 3874 (1983).

[21]M. Elahy and G. Dresselhaus, Phys. Rev. B **30**, 7225 (1984).

[22]D. G. Onn, M. G. Alexander, J. J. Ritsko, and S. Flandrois, J. Appl. Phys. **53**, 2751 (1982).

[23]M. Shayegan, M. S. Dresselhaus, L. Salamanca-Riba, G. Dresselhaus, J. Heremans, and J.-P. Issi, Phys. Rev. B **28**, 4799 (1983).

[24]M. K. Wilkinson, J. W. Cable, E. O. Wollan, and W. C. Koehler, Phys. Rev. **113**, 497 (1959).

[25]D. Billerey, C. Terrier, R. Mainard, and P. Meriel, C. R. Acad. Sci. (Paris) Ser. B **39**, 495 (1977).

[26]M. Suzuki, H. Ikeda, and Y. Endoh, Synth. Met. **8**, 43 (1983).

[27]M. Elahy, M. Shayegan, K. Y. Szeto, and G. Dresselhaus, Synth. Met. **8**, 35 (1983).

[28]H. Ikeda, Y. Endoh, and S. Mitsuda, J. Phys. Soc. Jpn. **54**, 3232 (1985).

[29]D. G. Wiesler, M. Suzuki, H. Zabel, S. M. Shapiro, and R. M. Nicklow, Physica **136B**, 22 (1986).

[30]M. Suzuki, D. G. Wiesler, P. C. Chow, and H. Zabel, J. Magn. Magn. Mater. **54-57**, 1275 (1986).

[31]S. Flandrois, J.-M. Masson, J.-C. Rouillon, J. Gaultier, and C. Hauw, Synth. Met. **3**, 1 (1981).

[32]G. K. Wertheim, Solid State Commun. **38**, 633 (1981).

[33]S. Flandrois, A. W. Hewat, C. Hauw, and R. H. Bragg, Synth. Met. **7**, 305 (1983).

[34]M. Matsuura, Y. Murakami, K. Takeda, H. Ikeda, and M. Suzuki, Synth. Met. **12**, 427 (1985).

[35]M. E. Lines, Phys. Rev. **131**, 546 (1963).

[36]D. G. Wiesler, M. Suzuki, P. C. Chow, and H. Zabel, Phys. Rev. B **34**, 7951 (1986).

[37]K. Katsumata and K. Yamasaka, J. Phys. Soc. Jpn. **34**, 346 (1973).

[38]P. A. Lindgård, R. J. Birgeneau, J. Als-Nielsen, and H. J. Guggenhiem, J. Phys. C **8**, 1059 (1975).

[39]M. Suzuki, K. Koga, and Y. Jinzaki, J. Phys. Soc. Jpn. **53**, 2745 (1984).

[40]See introductory texts; for example, Chap. 2 of G. L. Squires, *Introduction to the Theory of Thermal Neutron Scattering* (Cambridge University Press, Cambridge, 1978).

[41]W. Marshall and R. D. Lowde, Rep. Prog. Phys. **31**, 705 (1968).

[42]The present discussion follows the treatment found in the appendix of P. W. Stephens, P. A. Heiney, R. J. Birgeneau, P. M. Horn, D. E. Moncton, and G. S. Brown, Phys. Rev. B **29**, 3512 (1984). A different, but equivalent, formalism is presented by S. K. Sinha, in *Neutron Scattering,* edited by D. L. Price and K. Skold (Plenum, New York, in press), Chap. 9.

[43]M. J. Cooper and R. Nathans, Acta Crystallogr. Sect. A **24**, 481 (1968).

[44]S. Hendricks and E. Teller, J. Chem. Phys. **10**, 147 (1942).

[45]B. E. Warren, Phys. Rev. **59**, 693 (1941).

[46]The resolution width at Co(1,0,0) is taken as 89% of that at the G(1,0,0) peak, as expected from calculations of the resolution function for a double-axis neutron spectrometer with a Be monochromator and 60′-20′-20′ collimation, based on the treatment of Ref. 43.

[47]D. G. Wiesler and H. Zabel, Phys. Rev. B **36**, 7303 (1987).

[48]The magnetic form factor we utilized was based on a 15% reciprocal-space expansion of the spherically averaged values calculated by R. E. Watson and A. J. Freeman, Acta Crystallogr. **14**, 27 (1961). See also D. C. Khan and R. A. Erickson, Phys. Rev. B **1**, 2243 (1970).

[49]J. D. Axe and J. B. Hastings, Acta Crystallogr. Sect. A **39**, 593 (1983).

[50]P. Dutta and S. K. Sinha, Phys. Rev. Lett. **47**, 50 (1981).

[51]From tables of nuclear scattering lengths in *Dynamics of Solids and Liquids by Neutron Scattering,* edited by A. W. Lovesey and T. Springer (Springer, Berlin, 1977).